

# Sub-surface nuclear tests monitoring through the CTBT xenon network

Frédéric Hourdin<sup>1</sup>

Laboratoire de Mtorologie Dynamique du CNRS, IPSL, Paris, France

J.-P. Issartel<sup>1</sup>

Commissariat l'Energie Atomique, Centre d'Etude de Bruyres le Chtel, France

**Abstract.** We present the first evaluation of the atmospheric xenon network to be installed as part of the International Monitoring System (IMS) in the frame of the Comprehensive Test Ban Treaty (CTBT). We show that this network should, by itself, provide a significant contribution to the total efficiency of the IMS. For this evaluation, we introduce an inverse approach based upon the time symmetry of the atmospheric transport of trace species. This approach may find applications in a variety of environmental problems.

## Introduction

The Comprehensive Test Ban Treaty (C.T.B.T., *Sullivan, 1998, Garwin, 1997, De Geer, 1997*) verification will rely on an International Monitoring System (IMS) which should detect nuclear tests down to 1 kiloton (kt) TNT equivalent anywhere on the planet. The IMS is based upon four global networks. Seismic (*Richards et Won-Young, 1997, Barker et al., 1998*), hydroacoustic and infrasound waves will help check for underground, under-water and atmospheric nuclear tests. The fourth network will monitor atmospheric radionuclides. 80 stations will measure aerosols, released for atmospheric tests only, and a subset of 40 will additionally detect xenon isotopes. Insoluble in water, xenon is released in the atmosphere after under-water tests as well. It also exhales from underground tests through induced or natural faults (*De Geer, 1996, Carrigan, 1996*). With a half-life  $\tau = 5.2$  days,  $^{133}\text{Xe}$  is the dominant isotope at long distance. Estimation of the amount  $q$  of  $^{133}\text{Xe}$  effectively released after a 1 kt sub-surface test is a delicate matter. The CTBT Preparatory Commission agreed on the following scenario :  $q = 10^{15}$  Bq for evasive atmospheric/underwater and  $q = 10^{14}$  Bq for underground tests. In May 1998, the same commission decided which 40 out of the 80 radionuclide stations should be proposed to the Conference of States Parties for being equipped with noble gas detection capability. Specification for detection threshold is  $1 \text{ mBq m}^{-3}$  with air sampled over one day.

Based upon those specifications, we present an evaluation of  $^{133}\text{Xe}$  monitoring efficiency for sub-surface test

detection. Atmospheric dispersion is computed with the transport version of the atmospheric general circulation model of Laboratoire de Météorologie Dynamique, LMD-ZT. The model includes a finite volume transport scheme for large scale advection (*Van Leer, 1977, Hourdin et Armengaud, 1999*), a second order closure for turbulent mixing in the planetary boundary layer, as well as a mass flux representation of deep convection (*Tiedtke, 1989*). The 3.3 version we use essentially differs from the 2.2 presented by *Hourdin et Armengaud (1999)* by the use of an hybrid  $\sigma$ -pressure coordinate on the vertical. LMD-ZT is used in two modes. Firstly, meteorological simulations are performed with a horizontal resolution of  $3.8^\circ$  by  $2.5^\circ$  and 19 layers on the vertical. Winds and temperature are relaxed toward re-analysis of the European Center for Medium Range Weather Forecast with a time constant of 2.5 hours (nudging). Large scale winds, turbulent mixing coefficients and sub-grid scale convective mass fluxes are averaged in time and archived with a 6-hour sampling period. Meteorological archives were built for July 1990 and January 1991, in order to investigate seasonal effects. Secondly, the transport model is used "off-line" by reading these archives. The horizontal resolution is then twice as fine ( $1.9^\circ$  by  $1.25^\circ$ ).

Monitoring efficiency depends on test location and meteorological conditions. In order to reduce computation of relevant statistics to a practicable dimension, we use reverse transport computations: the radioactive tracer is transported back from the detector (one of the CTBT stations) and measured at the source (location of nuclear test), thus replacing all possible sources by 40 fictitious ones. This approach can be seen as a generalization of the classical back-tracking of air masses (*Hess et al., 1996, Ramonet et al., 1996*). Here, parameterizations of turbulent mixing and convective transport are inverted as well.

## Reciprocity of atmospheric transport

Let us idealize a nuclear test as the instantaneous release at time  $t_s$  in a volume  $S$  (in practice a grid-mesh of our numerical model) of an amount  $q$  of radionuclide. Detection will occur if the mean concentration in the detection mesh  $D$  (containing the CTBT station) at detection time  $t_D$  is above the threshold value. In fact, for a given meteorological sequence, this concentration is obtained as well in  $S$  at  $t_s$  by injecting  $q$  in  $D$  at  $t_D$  and reversing time in the transport computation. This reciprocity is illustrated in Fig. 1a in the case of pure advection.

Mathematically,  $\bar{c}(D, t_D) = \bar{c}^*(S, t_s)$  where “-” stands for volume average and where the direct and reverse tracern

<sup>1</sup>Authors contributed equally to the work

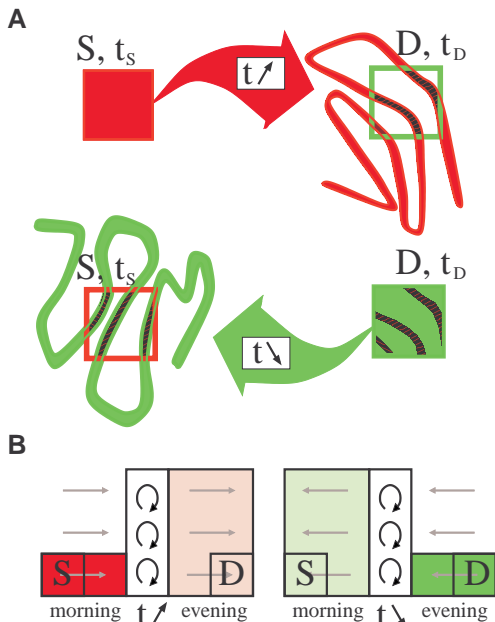


**Figure 1.** Illustrations of the reciprocity of atmospheric transport. **(A):** The radioactive tracer uniformly mixed at time  $t_s$  in S is reshaped as a filament (red) by advection. The air in D at  $t_D$  is the gathering of air coming from S (intersection with the red filament, shaded) and tracer-free air. When tracking single particles back in time from D at  $t_D$ , the particles in the shaded area come back in S whereas the other particles spread outside S (green filament). **(B):** Schematic view of the dilution of a pollutant injected near the surface due to a strong development of the convective planetary boundary layer at noon. Evening concentration in D is obtained as well as morning concentration in S if the tracer is transported backward from D and undergoes the same mixing at noon.

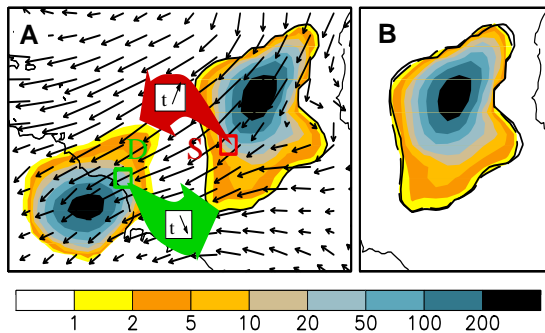


**Figure 2.** Example of visibility area computation. Source term:  $q = 10^{15}$  Bq. Colors:  $^{133}\text{Xe}$  concentration in  $\text{mBq kg}^{-1}$ . **(A)**, left cloud: direct computation with injection at 0:00 UT on January 15th 1991 in S. Concentrations are averaged on January 18th. **(A)**, right cloud: reverse computation with injection on January 18th in D (CTBT station located in Cayenne). Concentrations correspond to January 15th at 0:00 UT. The measurement is either the value inside the green square (forward estimation,  $\bar{c}(D, t_D) = 24 \text{ mBq kg}^{-1}$ ) or that in the red square (backward estimation,  $\bar{c}^*(S, t_s) = 28 \text{ mBq kg}^{-1}$ ). The  $1 \text{ mBq kg}^{-1}$  contour of the right cloud (black curve) gives the visibility of the station on January 18th for 1 kt tests on January 15th. **(B):** Direct estimation of the visibility area. Direct simulations are performed starting from each grid point on January 15th. The concentration in D on the 18th is reported to the source. The dashed curve delimits the corresponding visibility area. The full curve is the same as in **(A)**. Direct and reverse estimates almost coincide. Small differences are due to the lack of symmetry of the numerical schemes.

concentrations obey the following equations :

$$\frac{\partial c}{\partial t} + \vec{V} \cdot \text{grad } c + \lambda c = q \times \sigma(S, t_s) \quad (1)$$

and

$$-\frac{\partial c^*}{\partial t} - \vec{V} \cdot \text{grad } c^* + \lambda c^* = q \times \sigma(D, t_D) \quad (2)$$

$\vec{V}$  is the wind field (the same meteorological archive is read backward in the reverse computation),  $\lambda = \ln 2 / \tau$ , and the source function  $\sigma(S, t_s)$  is a dirac in time at  $t_s$  inside volume S divided by the mass of air inside the volume and 0 outside. The identity  $\bar{c}(D, t_D) = \bar{c}^*(S, t_s)$  arises from the fact that  $\frac{d}{dt} \int_{\Omega} \rho c c^* d\omega = 0$  for time  $t$  between  $t_s$  and  $t_D$ , strictly ( $\rho$  is the air density). This result is obtained from Eqs 1, 2 and atmospheric mass conservation after integration by part (tracer fluxes are assumed to be zero on the boundaries of the atmospheric domain  $\Omega$ ). From the same simple algebra, it can be shown also that Eq. 2 is the adjoint of Eq. 1 for scalar product  $(\phi, \psi) \rightarrow \int_{\Omega \times R} \rho \phi \psi d\omega dt$  where  $R$  is the time domain. So reverse and adjoint transport computations (see Pudykiewicz, 1998, for a use of adjoint computation in the CTBT context) are mathematically equivalent although the underlying views are generally associated with different inversion algorithms.

Applications of the reciprocity of atmospheric transport are generally restricted to back tracking of individual (Lagrangian) air particles accounting for large scale transport only (Hess *et al.*, 1996). In fact, Eulerian formulation can be kept for reverse computations. Moreover, reciprocity does extend to parameterizations of turbulent sub-grid scale advection. In practice, formal transformation of parameterizations must be performed carefully. In classical planetary boundary layer schemes, the turbulent mixing is accounted for with a diffusive operator  $\frac{1}{\rho} \frac{\partial}{\partial z} [K \rho \frac{\partial c}{\partial z}]$  on the right hand side of Eq. 1 (the schemes generally differ in the formulation for  $K$  which can be rather sophisticated). The underlying view consisting in mixing by small scale turbulent and symmetrical upward and downward motions implies an equivalent mixing in the reverse world (see illustration in Fig. 1b) which must be accounted for by the same self-adjoint operator  $\frac{1}{\rho} \frac{\partial}{\partial z} [K \rho \frac{\partial c^*}{\partial z}]$ , with same sign, in Eq. 2. On another hand

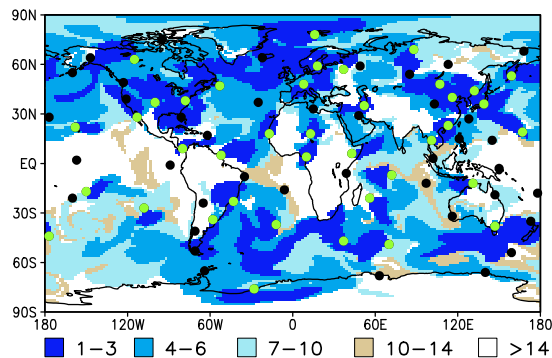


**Figure 3.** Detection delay (in days) of the xenon sub-network for a 1 kt sub-surface test on January 15th 1991. The entire colored area is the visibility after 14 days. Green dots are the corresponding stations. Black dots are the other 40 stations of the radionuclide network.

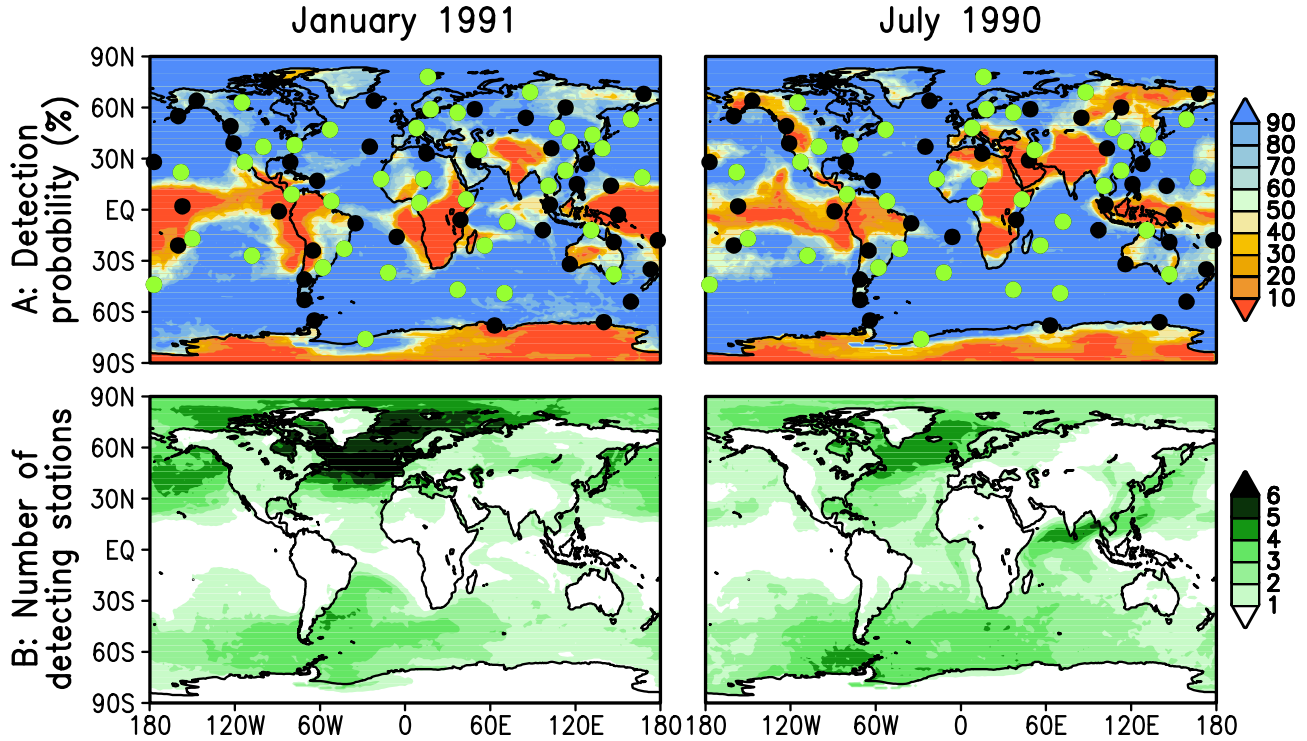


**Figure 4.** Efficiency of the xenon sub-network for 1 kt sub-surface tests. (A) : detection probability (%). (B) : average number of independent stations detecting a test.

for deep convection parameterizations where concentrated updrafts can be balanced by much slower sinking in the environment, signs of the convective fluxes must be changed : in the reverse computation, the tracer goes up slowly in the environment and comes back to the surface much faster in the center of the convective tower.

As in the direct world, reverse large scale transport (Fig. 1a) or turbulent mixing (Fig. 1b) both broaden source areas. Indeed molecules which have gathered in D at  $t_D$  come from a region the size of which increases with elapsed time. Radioactive decay in the direct world corresponds to an equivalent decay in the past. Finally, one-day sampling at the detector is accounted for in the reverse world by emitting the tracer uniformly over one day.

## Results and discussion

For a station D and for given dates  $t_S$  and  $t_D$ , one single reverse model integration provides the station visibility defined as the area from which a 1 kt test at  $t_S$  would be detected in D at  $t_D$  (concentration above the  $1 \text{ mBq m}^{-3}$  threshold, illustration in Fig. 2). In order to evaluate a network efficiency, Prinn (1988) defined an “effectively sampled region” based upon perturbation of a steady state advective-diffusive equation accounting for the typical wind intensity and diffusion coefficient at the station. Although based on similar concepts, our visibility area is a binary determination of the monitored area for a specific meteorological sequence.

For a given date  $t_S$  of the nuclear event, we further define the global network visibility after  $N$  days as the gathering of the visibility of all stations for all measurements happening

within  $N$  days after the event. An example of global visibility map is given in Fig. 3. Detections typically occur several days after the test. The gain after 10 days is very weak. Finally, binary visibility maps for successive test dates  $t_S$  are averaged into detection probability maps. Probability maps after 14 days for July and January are shown in Fig. 4.

Monitoring of atmospheric radioactivity by itself offers a good coverage of mid-latitudes due to efficient mixing by transient eddies, especially in southern hemisphere where 5 stations only offer more than 90% detection probability in the 30-60 S latitude band. In the 30-60 N latitude band, the seasonal cycle of transient activity is stronger: the number of stations detecting an oceanic test goes from 3-6 during winter (maximum activity) to 2-4 in summer. At this season, significant gaps appear on continents due to the weaker source term. In the intertropical zone, winds are more regular. The area monitored by an individual station often reduces to a narrow strip up-stream. Tracers are also efficiently removed from the lower troposphere by convection and ascending motions in the Inter Tropical Convergence Zone, especially on continents during summer. The weak network redundancy emphasizes the difficulty of choosing 40 stations in such a way that the network performs its duty everywhere.

Detection probability maps can not be directly validated against observations. However, the same model with same meteorological archives led to reasonably good agreements with observations for  $^{222}\text{radon}$ , comparable to those obtained by Mahowald, *et al.* (1997). Computations with different model resolutions and for different years do not alter the above conclusions, neither the good global coverage nor the location of gaps. Besides network evaluation, the

approach and tools presented here can help localize sources as will be shown in a forthcoming publication.

**Acknowledgments.** This study was funded by Commissariat l'Energie Atomique and Centre National de la Recherche Scientifique. Graphics have been made with the user friendly and public domain graphical package named GrADS originally developed by Brian Dotty (COLA, support@grads.iges.org) and maintained with the help of Mike Fiorino (LLNL).

## References

- B. Barker et al., Monitoring nuclear tests, *Science* 281, 1967–1968, 1998.
- C. R. Carrigan, R. A. Heinle, G. B. Hudson, J. J. Nitao, J. J. Zucca, Trace gas emissions on geological faults as indicators of underground nuclear testing, *Nature* 382, 528–531, 1996.
- L.-E. De Geer, Sniffing out clandestine tests, *Nature* 382, 491–492, 1996.
- L. Garwin, NRC backs open access to test-ban data, *Nature* 388, 107, 1997.
- P. G. Hess, N. Srimani, S. J. Flocke, Trajectories and related variations in the chemical composition of air for the Mauna Loa Observatory during 1991 and 1992, *J. Geophys. Res.* 101, 14,543–14,568, 1996.
- F. Hourdin and A. Armengaud, Test of a hierarchy of finite-volume schemes for transport of trace species in an atmospheric general circulation model, *Mon. Weather Rev.*, 127, 822–837, 1999.
- N. M. Mahowald, P. J. Rasch, B. E. Eaton, S. Whittlestone, R. G. Prinn, Transport of  $^{222}\text{Rn}$  to the remote troposphere using the Model of Atmospheric Transport and Chemistry and assimilated winds from ECMWF and the National Center for Environmental Prediction/NCAR, *J. Geophys. Res.*, 102, 28,139–28,151, 1997.
- J. T. Merrill, Isentropic airflow probability analysis, *J. Geophys. Res.*, 99, D12, 25,881–25,889, 1994.
- R. G. Prinn, Toward an improved global network for determination of tropospheric ozone climatology trends, *J. Atmos. Chem.* 6, 281–298, 1988.
- J. A. Pudykiewicz, Application of adjoint tracer transport equations for evaluating source parameters, *Atmos. Environ.* 32, 3039–3050, 1998.
- M. Ramonet, J. C. Le Roulley, P. Bousquet, P. Monfray, Radon-222 measurements during the Tropoz II campaign and comparison with a global atmospheric transport model, *J. Atmos. Chem.* 23, 107–136, 1996.
- Richards and K. Won-Young *Nature* 389, 781–782, 1997.
- J. D. Sullivan, The comprehensive test ban treaty, *Physics Today March*, 24–29, 1998.
- M. A. Tiedtke, A comprehensive mass flux scheme for cumulus parameterization in large-scale models, *Mon. Weather Rev.* 117, 1179–1800, 1989.
- B. Van Leer, Towards the ultimate conservative difference scheme : IV. A new approach to numerical convection, *J. Comput. Phys.* 23, 276–299, 1977.

---

F. Hourdin, LMD/CNRS/IPSL, UPMC, Boite 99, Tr 25-15, 5eme etage, Jussieu, F-75252 Paris Cedex 05 - France (e-mail: Frederic.Hourdin@lmd.jussieu.fr)

J.-P. Issartel, Centre d'Etude de Brueres-le-Chitel, CEA, France. (e-mail: issartel@ldg.bruyeres.cea.fr)

(Received July 13, 1999; revised November 22, 1999; accepted March 29, 2000.)